

Article

Carbon Membranes Prepared from Poly (Furfuryl Alcohol–Furfural) Precursors: Effect of FeCl₃ Additive

Areti Zaharopoulou ^{1,2}, Spyros N. Yannopoulos ¹  and Theophilos Ioannides ^{1,*} 

¹ Foundation for Research & Technology-Hellas, Institute of Chemical Engineering Sciences (FORTH/ICE-HT), 26504 Patras, Greece; a.zaharopoulou@iceht.forth.gr (A.Z.); sny@iceht.forth.gr (S.N.Y.)

² Department of Chemistry, University of Patras, 26504 Patras, Greece

* Correspondence: theo@iceht.forth.gr

Received: 10 July 2020; Accepted: 18 August 2020; Published: 21 August 2020



Abstract: Thermosetting resins, such as poly (furfuryl alcohol), are efficient precursors for preparation of carbon membranes with molecular sieving properties. Polymerization of furfuryl alcohol is catalyzed by Bronsted or Lewis acids. FeCl₃, showing Lewis-acid behavior, is an interesting polymerization catalyst, because it gets reduced into metallic iron during pyrolysis of the resin, promoting transformation of amorphous carbon into graphitic domains. The goal of the present work was to examine whether use of FeCl₃ as a polymerization catalyst of furfuryl alcohol–furfural mixtures could lead to preparation of carbon membranes with improved gas separation performance compared to those prepared with use of p-toluenesulfonic acid. The resins were deposited onto tubular porous ceramic supports and pyrolyzed at temperatures in the range of 500–1000 °C. Material characterization was carried out by X-Ray Diffraction, N₂ physisorption, Raman spectroscopy and Scanning Electron Microscopy. The membrane performance was examined using H₂, CO₂ and CH₄ as probe molecules. It was found that the membranes operate mainly via the molecular sieving mechanism and the use of FeCl₃ instead of p-toluenesulfonic acid does not lead to an improvement in the permeation characteristics of the respective membranes.

Keywords: carbon membrane; hydrogen; carbon dioxide; methane; furfuryl alcohol; furfural; permeation

1. Introduction

Carbon membranes are usually prepared by pyrolyzing a polymeric material under inert atmosphere or vacuum. Numerous precursors have been used for carbon membrane preparation such as thermosetting resin, graphite, coal, pitch and biomass [1,2]. Generally, the steps that have to be followed in order to prepare a carbon membrane are: precursor selection, polymeric membrane preparation, pretreatment, pyrolysis/carbonization, post treatment of the pyrolyzed membrane and module construction [1]. Carbon membranes can act as Carbogenic/(Carbon) Molecular Sieving (CMS) materials or as Selective Surface Flow Materials depending on the mechanism for the gas component separation. As for CMS membranes, the separation takes place due to differences in shape and size of the molecules in question [1,3], whereas the selectivity of Selective Surface Flow membranes is determined by preferential adsorption of certain components on the surface of the membrane pores, followed by selective diffusion of these components [4].

The most important step in carbon membrane preparation is the step of pyrolysis during which the pore structure of the membrane is created/developed and, as a consequence, the adsorption capacity and the gas separation properties are determined. Among the parameters that have to be controlled at this step, are pyrolysis temperature, time and flow rate of the purge gas. In addition, the pore structure of CMS membranes depends on the structure and configuration of the polymer precursor [5,6] whereas

the structural changes that the polymer undergoes during pyrolysis are not fully understood. In order to prepare a molecular sieve permselective membrane, the precursor must lead to the creation of pores with molecular dimensions.

Polyfurfuryl alcohol (PFA) is a suitable precursor of carbon membranes that exhibit a molecular sieving effect [7]. The corresponding aldehyde, furfural, polymerizes towards a black, cross-linked resin product [8]. Carbon materials produced by pyrolysis of resins derived from furfuryl alcohol–furfural mixtures are in the category of “glassy carbon” with a microtexture of turbostratic stacks of small polynuclear aromatic molecular fragments held together with random orientation by cross-linking [9]. Moreover, it has been proven that the formation of aromatic units appears at 400 °C and that porosity starts to appear after pyrolysis at 500 °C [9].

PFA-derived carbon membranes on different supports have been the subject of a number of studies. Sedigh et al. [10] developed and characterized PFA-derived CMS membranes on alumina tubular supports and measured their performance in the permeation of H₂, CO₂, CO, CH₄ and Ar as well as of CO₂/CH₄ binary mixtures and mixtures of H₂, CO₂, CO and CH₄. They found that the single gas permeation order was H₂ > CO₂ > CO > Ar, whereas in a H₂-CO₂-CO-CH₄ gas mixture the gas permeation order was CO₂ > H₂ > CO > CH₄, attributing this behavior to preferable adsorption of CO₂. Wang et al. [11] prepared CMS membranes on alumina tubular supports from PFA (PFA was prepared via vapor deposition polymerization) via pyrolysis at temperatures of 450, 525 and 600 °C and found that gas permeance increases with pyrolysis temperature. Song et al. [12] studied the permeation of H₂, CO₂, O₂, N₂ and CH₄ through carbon membranes synthesized from PFA on a carbon-based tubular support and concluded that gas separation is governed by a molecular sieving effect. Gas permeance decreases with the increase in pyrolysis temperature from 600 to 900 °C, while it increases with the increase in permeation temperature indicative of activated diffusion. Shiflett et al. [13] used the technique of ultrasonic deposition to synthesize microporous carbon membranes on stainless steel supports in order to achieve control over the deposition step.

In the present work, the effect of two different polymerization catalysts on the properties of the resulting carbon membrane has been studied. The two catalysts are p-toluenesulfonic acid (pTS) and FeCl₃, which decomposes to iron oxides and finally to metallic iron during pyrolysis. The precursor is a resin made from a mixture of furfuryl alcohol and furfural. Both precursors have thermosetting properties, making them proper materials for preparing carbon membranes as they do not fuse or melt after heating, whereas they retain structural shape during heating and pyrolysis. Moreover, they have high carbon content and they achieve high carbon yield after carbonization. Metallic iron, produced during pyrolysis via carbothermal reduction of Fe precursor, acts as a graphitization catalyst enhancing structural modifications of the resulting carbon membrane.

2. Materials and Methods

2.1. Carbon Membrane Preparation

Carbon membranes were synthesized on porous tubular ceramic supports (CTI, France) with external diameter of 8.5 mm, 5.5 cm length, 150 nm pore size and 40% porosity. Carbon membranes were synthesized using the following procedure: Two precursor solutions were prepared containing 2.3 mL furfural, 1 mL furfuryl alcohol, 7 mL acetone and either 50 mg p-toluenesulfonic acid (Solution_1) or 90 mg FeCl₃ (Solution_2) as polymerization catalysts. Firstly, the solid materials/components were dissolved in acetone and then the two polymeric precursor materials were added. Tubes named C1-TS and C2-Fe were immersed in Solution_1 and Solution_2, respectively, for 30 min, and after exposure in the atmosphere for 15 min, they were sealed in a bottle and treated at 90 °C for at least 24 h in order for polymerization to take place. Subsequently, the coated tubes were pyrolyzed at 500–1000 °C for 1 h under nitrogen flow so as to obtain the carbon membrane. Successive coating/pyrolysis cycles were employed for each sample. Following each carbonization cycle, the performance of the two carbon membranes (Sample C1-TS and C2-Fe) was evaluated by single gas permeation measurements of H₂,

CH₄ and CO₂ using the Wicke–Kallenbach method. The poly (furfuryl alcohol–furfural) membranes obtained after treatment at 90 °C were impermeable to hydrogen, carbon dioxide and methane.

2.2. Membrane Characterization

Following the same procedure as the one employed for membrane synthesis, free standing carbon powders were prepared and their structural and morphological properties were characterized by X-ray diffraction (XRD), N₂ physisorption and Raman spectroscopy. More specifically, carbon powders were prepared by pyrolysis at 500, 700, 800, 900 and 1000 °C for 1 h under nitrogen (N₂) flow.

XRD patterns were obtained on a Bruker D-8 ADVANCE diffractometer (Bruker Corporation, Billerica, MA, USA) equipped with a LynxEye position sensitive detector, using a Cu K α X-ray source (40 kV, 40 mA).

N₂ physisorption measurements were obtained at the Autosorb-1 instrument (Quantachrome, Anton Paar GmbH, Graz, Austria). The samples were degassed for at least 2 h at 250 °C before measurement. The specific area was calculated by the Brunauer–Emmett–Teller (BET) equation in the pressure range (p/p_0) of 0.05–0.3 and the total pore volume at p/p_0 value of 0.995–0.998.

Raman spectra were recorded by a near-UV Raman spectrometer (Labram HR-800, Horiba Jobin-Yvon, Edison, NJ, USA). Spectra were excited with the 441.6 nm line emerging from an air-cooled HeCd laser. The laser was focused on the sample with 50 \times objective lens (NA = 0.55) through a microscope. The scattered light was then collected in a backscattered geometry and analyzed by a single monochromator and registered by a Charge-Coupled Device (CCD). The spectral resolution was 2.5 cm⁻¹ and the integration time for the spectra was 200 s.

2.3. Gas Permeation Measurements

Gas permeation measurements were carried out as a function of pyrolysis temperature, permeation temperature and feed mixture compositions in a Wicke–Kallenbach set-up. The permeance of H₂, CO₂ and CH₄ as single components and H₂–CO₂ binary mixtures were measured using He as sweep gas. All gaseous flows were adjusted using mass flow controllers (Aera FC-7700C, Hitachi Metals Europe, Duesseldorf, Germany). The feed and sweep flow rates were 50 cm³ min⁻¹. The pressure on both sides, feed and permeate, was kept atmospheric. The gas composition at the permeate side was determined using a gas chromatograph (GC-2014, Shimadzu, Kyoto, Japan) equipped with a thermal conductivity detector (TCD).

3. Results

3.1. XRD Analysis

XRD patterns of C1-TS sample prepared by pyrolysis at temperatures between 500 and 1000 °C are presented in Figure 1. The patterns are characterized by broad peaks in the 15–30° and 40–50° regions, indicative of absence of long-range crystallinity. Peaks become larger with the increase in pyrolysis temperature. The pattern of sample C1-TS pyrolyzed at 500 °C contains a shoulder at ~13°, which disappears at higher pyrolysis temperatures. Such a feature could be attributed to the presence of oxygenated species in an analogous manner to graphene or graphite oxide.

The lateral size (L_a) and stacking height (L_c) of graphite nanocrystallites was calculated from XRD patterns via the following Equations (1) and (2).

$$L_a = 1.84 \lambda / (B_a \cos \varphi_a) \quad (1)$$

$$L_c = 0.89 \lambda / (B_c \cos \varphi_c) \quad (2)$$

where λ is the wavelength of the employed X-ray, B_a and B_c are the widths at half maximum of (100) and (002) graphite peaks, and φ_a and φ_c are the corresponding diffraction angles. The corresponding

regions in the XRD patterns were deconvoluted with XPSPEAK, Version 4.1 software (Informer Technologies, Inc. Developer: Raymund Kwok).

The $d(002)$ spacing of nanocrystalline graphite has been calculated by Bragg's equation.

$$d = \lambda / (2 \sin \theta) \quad (3)$$

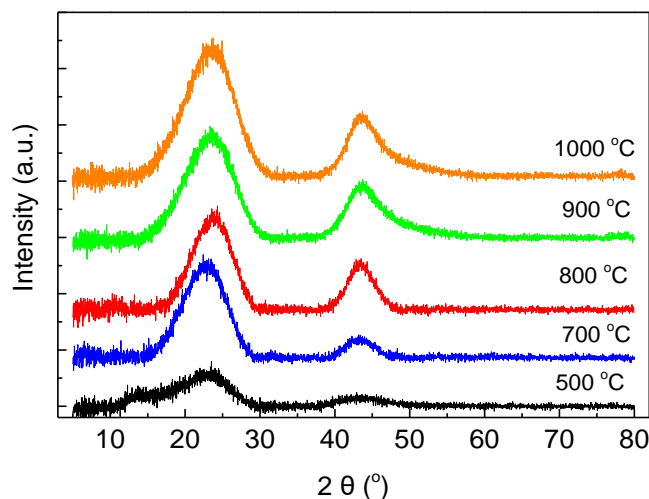


Figure 1. XRD patterns of sample C1-TS pyrolyzed at 500, 700, 800, 900 and 1000 °C.

Table 1 presents the parameter values calculated from Equations (1)–(3) for sample C1-TS, which has been prepared from the corresponding resin by pyrolysis at 700–1000 °C. Parameter values could not be obtained from the corresponding XRD pattern of the sample pyrolyzed at 500 °C due to its essentially amorphous nature. The $d(002)$ interlayer spacing is in the range of 0.351–0.363 nm for all samples, which is greater than the value of 0.335 nm corresponding to crystalline graphite. The stacking height, L_c , which indicates the crystallite size along the c axis, does not vary considerably and is in the range of 1.64–1.84 nm. This corresponds to an average number of layers stacking in coherent regions equal to five. The lateral size, L_a , is in the range of 4.18–5.54 nm and appears to increase slightly at the highest pyrolysis temperature employed. The obtained L_a and L_c values are quite low and correspond to highly disordered carbon material. The increase in pyrolysis temperature does not seem to affect significantly the dimensions of these domains, but rather their number density.

Table 1. Structural parameters calculated from XRD patterns of the C1-TS sample prepared using pTS catalyst.

Pyrolysis Temp (°C)	Lateral Size (L_a) nm	Stacking Height (L_c) nm	$d(002)$ nm
700	na	1.78	0.361
800	4.48	1.86	0.351
900	4.18	1.64	0.363
1000	5.54	1.84	0.355

The corresponding XRD patterns of C2-Fe samples pyrolyzed at 500–1000 °C are shown in Figure 2. The crystalline phase of magnetite (Fe_3O_4) is present after pyrolysis at 500 °C. At higher pyrolysis temperatures, magnetite is reduced to metallic iron ($2\theta = 45^\circ$), which catalyzes the graphitization of carbon, as evidenced by the growth of the (002) ($2\theta = 26^\circ$) graphite peak. In addition, the cohenite (Fe_3C) crystalline phase is formed after pyrolysis at 700 °C, whereas small peaks of iron carbide are also present at higher pyrolysis temperatures. The intensity of the graphite (002) peak increases with the increase in pyrolysis temperature from 700 to 1000 °C. The use of FeCl_3 as a catalyst during resin

synthesis leads, therefore, to the formation of metallic iron during pyrolysis and, as a result, to the creation of graphitic structures, probably in the vicinity of iron crystallites.

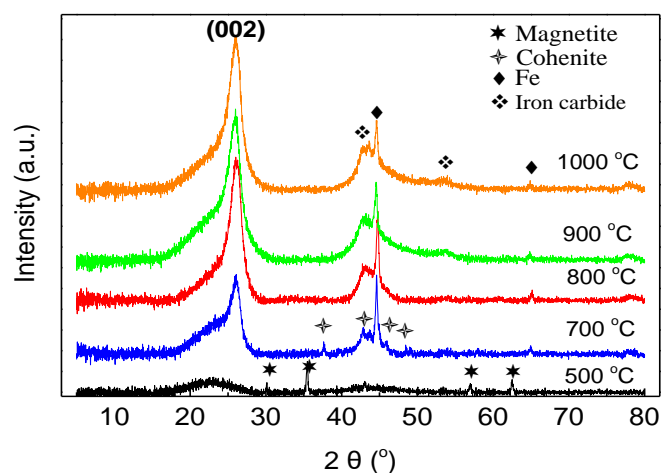


Figure 2. XRD patterns of sample C2-Fe pyrolyzed at 500, 700, 800, 900 and 1000 °C.

Table 2 presents the parameter values calculated from Equations (1)–(3) for sample C2-Fe, which has been prepared from the FeCl_3 -containing resin by pyrolysis at 700–1000 °C. Parameter values could not be obtained from the corresponding XRD pattern of sample pyrolyzed at 500 °C due to its essentially amorphous nature. The $d(002)$ interlayer spacing is in the range of 0.341–0.344 nm for all samples, which is slightly greater than the value of 0.335 nm corresponding to crystalline graphite, but smaller than the values for the C1-TS sample. The stacking height, L_c , which indicates the crystallite size along the c axis, does not vary considerably and is in the range of 4.66–5.52 nm. This corresponds to an average number of layers stacking in coherent regions higher than 13. The lateral size, L_a , is in the range of 14.60–19.63 nm and does not show a specific trend with pyrolysis temperature. The obtained L_a and L_c values are higher than the ones observed over the C1-TS sample, which is indicative of a more ordered carbon material. The increase in pyrolysis temperature does not seem to affect significantly the dimensions of these domains, but rather their number density.

Table 2. Structural parameters calculated from XRD patterns of the C2-Fe sample prepared using FeCl_3 catalyst.

Pyrolysis Temp (°C)	Lateral Size (L_a) nm	Stacking Height (L_c) nm	$d(002)$ nm
700	-	5.52	0.342
800	19.63	4.92	0.341
900	14.60	4.66	0.344
1000	17.93	4.69	0.343

3.2. Nitrogen Physisorption

The N_2 physisorption isotherms for sample C1-TS pyrolyzed at 800 °C and 900 °C are shown in Figure 3. The isotherms are characterized by wide, open-loop adsorption–desorption branches (I and II type) and of type H4 hysteresis loop [14]. The presence of the open hysteresis loop is evidence of the microporous structure of narrow slit-like pores [15].

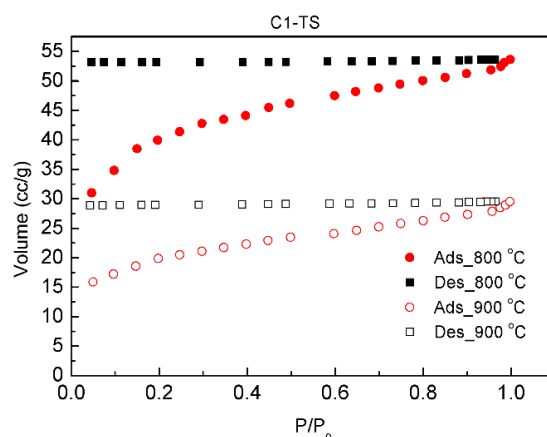


Figure 3. N₂ physisorption isotherms for sample C1-TS pyrolyzed at 800 °C and 900 °C.

The N₂ physisorption isotherms for sample C2-Fe pyrolyzed at 500 °C and 800 °C are shown in Figure 4. The observed isotherms are of type II (500 °C) and IV (800 °C) and, similarly to sample C1-TS, are characterized by open-loop adsorption–desorption branches, which, however, are less wide than those of the C1-TS sample, indicating the existence of micropores and mesopores. The observed hysteresis is of type H2 and at $p/p_0 = 0.42$ the opening of the hysteresis loop becomes smaller as the desorption curve falls rapidly and tends to approach the adsorption branch. It is worth noting that, for both samples, the hysteresis extends to low p/p_0 values, which is indicative of non-reversible adsorption of nitrogen in ultra-small pores, with size comparable to the size of the N₂ molecule [9].

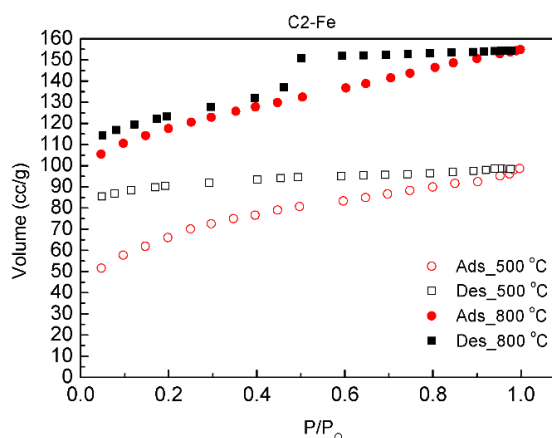


Figure 4. N₂ physisorption isotherms for sample C2-Fe pyrolyzed at 500 °C and 800 °C.

Table 3 presents the specific surface area (SSA), the total pore volume and the micropore volume as calculated using the adsorption/desorption isotherms for both samples. It is noted that the micropore volume was calculated using the t-plot method and de-Boer equation.

Table 3. Structural parameters calculated from nitrogen physisorption isotherms.

Pyrolysis Temperature (°C)	Specific Surface Area (m ² g ⁻¹)		Pore Volume (cm ³ g ⁻¹)			
	C1-TS	C2-Fe	Total		Micropore	
			C1-TS	C2-Fe	C1-TS	C2-Fe
500	2	226	0.002	0.0002	0.15	0.12
700	135	395	0.08	0.07	0.22	0.20
800	138	389	0.08	0.07	0.24	0.215
900	68	375	0.05	0.036	0.23	0.21
1000	11	325	0.01	0.008	0.21	0.18

As shown in Table 3, sample C1-TS does not have a porous structure after pyrolysis at 500 °C, the calculated specific area is only 2 m² g⁻¹ and pore volume is 0.0002 cm³ g⁻¹. On the other hand, sample C2-Fe after pyrolysis at the same temperature has developed a porous structure with a SSA of 226 m² g⁻¹ and a pore volume of 0.15 cm³ g⁻¹. The SSA of sample C1-TS is maximized (135–138 m² g⁻¹) after pyrolysis at 700 or 800 °C, while the maximum SSA (395 m² g⁻¹) of the C2-Fe sample is obtained after pyrolysis at 700 °C. Fitzer et al. [9] have reported that, during synthesis of glassy carbon from a polyfurfuryl alcohol precursor, the maximum specific surface area appears after pyrolysis at 700 °C. Comparing the micropore volume with the total pore volume, it is concluded that the micropore volume amounts to 70–88% of the total for sample C1-TS and to 83–91% of the total for sample C2-Fe.

As stated above, the presence of open-loop hysteresis for both samples suggests that the pore size is similar to that of the N₂ molecule. In sample C2-Fe, the pores are grown up after pyrolysis at 500 °C, whereas for sample C1-TS after 700 °C. Moreover, the presence of Fe favors the creation of mesopores. The maximum specific surface area for sample C1-TS was ~ three times smaller than that for sample C2-Fe, confirming the fact that the presence of Fe promotes the development of a porous structure.

3.3. SEM Analysis

The cross-sectional and top-view images of the C1-TS membrane obtained after 17 coating cycles and a pyrolysis temperature of 1000 °C are shown in Figure 5, while the cross-sectional and top-view images of C2-Fe membrane obtained after 19 coating cycles and a pyrolysis temperature of 1000 °C are shown in Figure 6. The SEM images reveal a carbon layer with a thickness of about 2 μm deposited on the tubular support in the case of the C1-TS membrane. The carbon layer is not as readily visible in the case of the C2-Fe membrane, because of more extensive penetration of the deposited layers inside the porous structure of the support. Comparing the top-view images of sample C1-TS and sample C2-Fe, the presence of Fe particles, with size in the range 150–300 nm, is evident in the latter case.

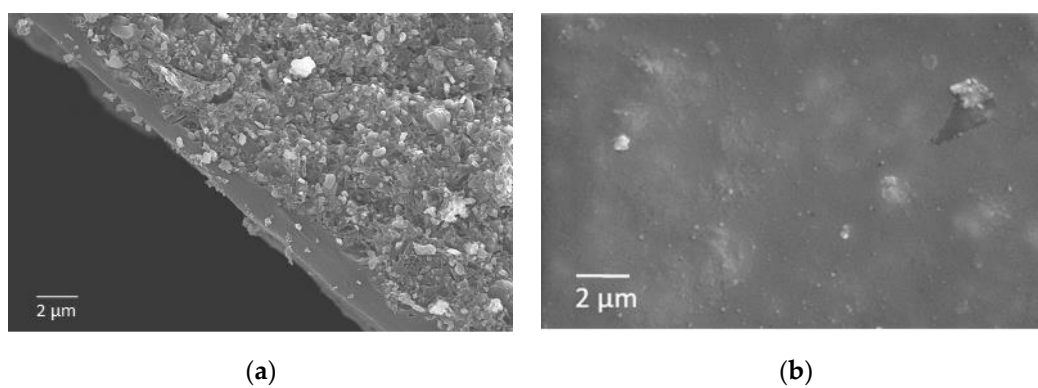


Figure 5. (a-left): cross-sectional and (b-right) top-view images of Sample C1-TS after 17 coating cycles and a pyrolysis temperature of 1000 °C.

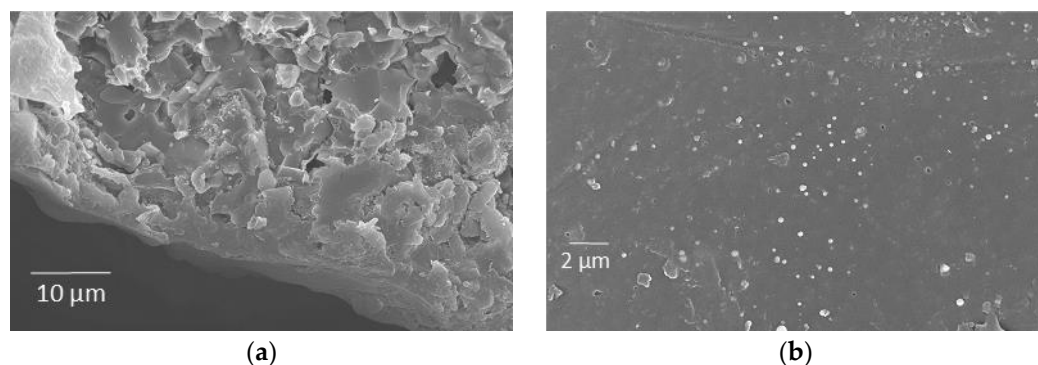


Figure 6. (a-left) cross-sectional and (b-right) top-view images of Sample C2-Fe after 19 coating cycles and a pyrolysis temperature of 1000 °C.

3.4. Raman Spectroscopy

Raman spectroscopy has been proven a versatile technique in studies of carbon-based materials, providing information on crystallinity, defects and disorder; hence, being able to distinguish various graphitic forms. The sp^2 carbon networks of graphite-type materials are characterized by a prominent doubly degenerate (E_{2g} symmetry) G-band at $\sim 1582\text{ cm}^{-1}$ originating from the in-plane bond-stretching motion. [16,17]. The Raman spectrum changes appreciably when the crystal size decreases down to the nanometer scale as the D-band appears at $\sim 1350\text{ cm}^{-1}$ for visible excitation. The D-band is not Raman active in a perfect, defect-free sp^2 lattice and corresponds to the breathing mode of the sp^2 rings.

Tuinstra and Koenig [18] were the first to show that the D-band intensity depends upon the crystallite size. They combined Raman and XRD data of several graphitic samples with different crystallite sizes L_a , (in-plane correlation length) and found that the intensity (peak height) ratio of the D and G bands is given by

$$\frac{I(D)}{I(G)} = \frac{C(\lambda)}{L_a} \quad (4)$$

where $C(\lambda)$ is an excitation wavelength-dependent factor; e.g., $C(514.5\text{ nm}) \approx 44\text{ \AA}$. This model assumes a uniform breakdown of graphite to nanocrystals and has been verified for a minimum of $L_a \approx 2\text{ \AA}$. Later, it was shown [19] that the D/G band intensity ratio strongly depends on the excitation wavelength according to the relation

$$L_a(\text{nm}) = (2.4 \times 10^{-10}) \lambda_{\text{laser}}^4 (A(D)/A(G))^{-1} \quad (5)$$

where A denotes the integrated Raman peak area.

Representative Raman spectra of the pyrolyzed materials are shown in Figure 7. The spectra are composed of broad and overlapping G and D bands. To estimate the influence of the pyrolysis temperature on the crystallite size L_a , using the above relation, the Raman bands have been deconvoluted into Gaussian lines, as shown in Figure 7. Apart from the G and D bands, as denoted by hatched areas, two additional bands are needed for a reliable fitting of the experimental Raman spectra. These bands, denoted by dashed lines, are located at $\sim 1200\text{ cm}^{-1}$ and 1550 cm^{-1} . Their frequencies are used as free fitting parameters and are scattered by less than $\pm 10\text{ cm}^{-1}$ from the above values for the various Raman spectra. These two bands originate possibly from residuals of the pyrolysis process. The band at $\sim 1200\text{ cm}^{-1}$ has been assigned to a combination of vinylene and C-H in-plane deformations while the band at $\sim 1550\text{ cm}^{-1}$ arises from the stretch of furan rings [20]. The situation is a bit more complicated for the C2-Fe Raman spectra shown in Figure 7b, where a reliable band fitting necessitates the use of an additional weak peak, superimposed on the wide D-band. This is more evident for the spectra that correspond to 700, 900, and 1000 °C pyrolysis temperatures. The energy and narrow width of this band testify towards its graphitic origin. The formation of a graphitic phase dispersed in the nanocrystalline/amorphous carbon phase is in agreement with the XRD results that revealed a graphitic phase surrounding Fe nanoparticles.

Ferrari and Robertson proposed a detailed a three-stage mechanism about how the increase in disorder leading from graphite to amorphous carbon affects the spectral features of the Raman bands [16]. They considered that the Raman spectrum depends upon the following factors: (i) clustering of the sp^2 phase, (ii) bond disorder, (iii) presence of sp^2 rings or chains, and (iv) the sp^2/sp^3 ratio. In the first stage (I), where graphite turns to nanocrystalline graphite, no sp^3 sites are still created and the G-band shifts from $\sim 1582\text{ cm}^{-1}$ to $\sim 1600\text{ cm}^{-1}$. In this regime, the intensity ratio $I(D)/I(G)$ follows the Tuinstra–Koenig prediction [18]. In the second stage (II), the further increase in defects will turn nanocrystalline graphite to mainly amorphous sp^2 bonded carbon. In Raman spectra, one observes a shift of the G-band to lower wavenumbers, the Tuinstra–Koenig relation fails and the intensity ratio $I(D)/I(G)$ decreases.

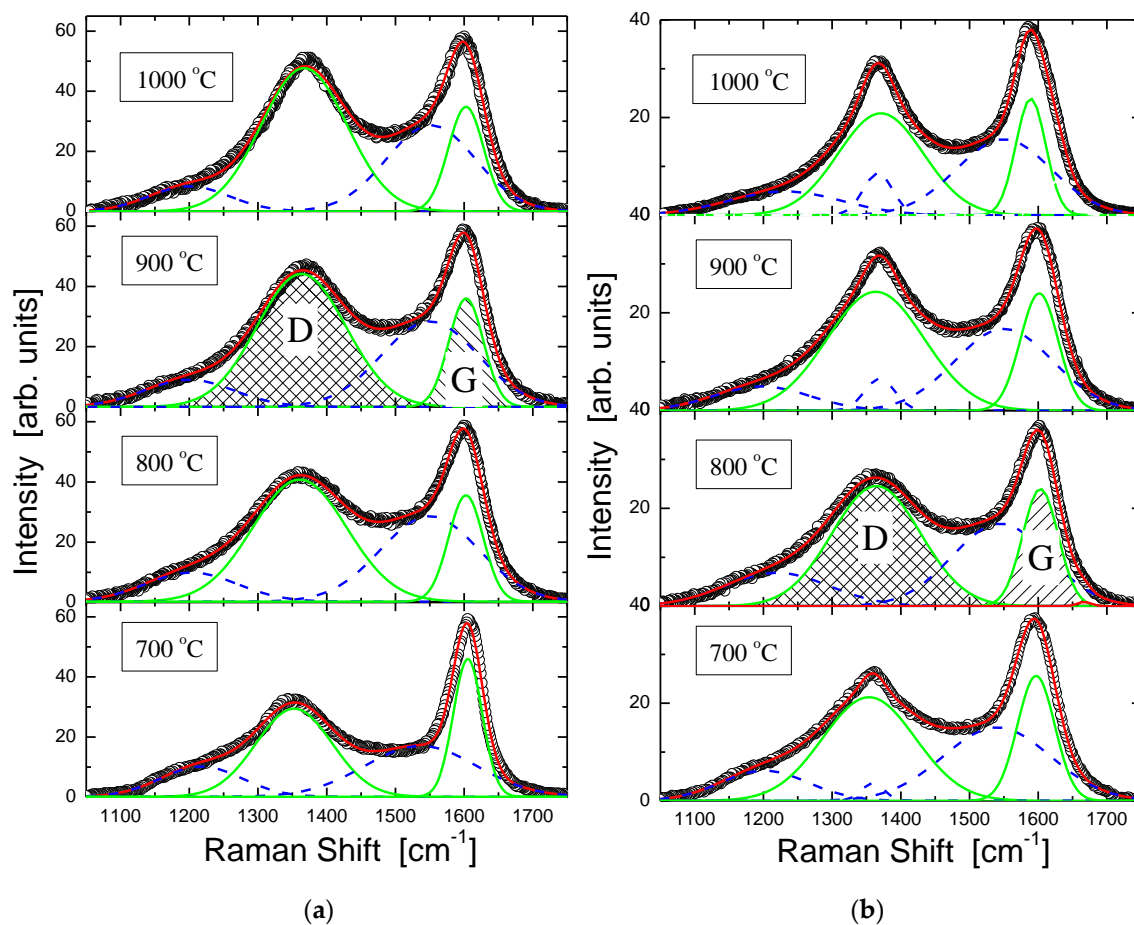


Figure 7. Gaussian line fitting of the Stokes-side Raman spectra of (a) C1-TS and (b) C2-Fe at various pyrolysis temperatures. The open circles correspond to the experimental points, while the thick line passing through the points is the best fit result.

Figure 8a,b illustrate the dependence of various spectral parameters of the G and D bands as a function of the treatment temperature for C1-TS and C2-Fe, respectively. The following observations emerge from these results. (i) The G-band frequency is located at $\sim 1600 \pm 2 \text{ cm}^{-1}$ for both systems and for all temperatures of pyrolysis, apart from the highest one for the C2-Fe, where it shows a slight red-shift to 1590 cm^{-1} . In the frame of the Ferrari–Robertson model, the G-band energy at $\sim 1600 \text{ cm}^{-1}$ shows that pyrolysis produces nanocrystalline graphite (stage I of the model), while the small red-shift to 1589 cm^{-1} at 1000 °C heralds the incipient transformation of nanocrystalline graphite to mainly amorphous sp^2 bonded carbon (stage II of the model). (ii) The D-band frequency increases systematically with increasing pyrolysis temperature for both C1-TS and C2-Fe. (iii) The full width of the D and G bands follows a common trend, namely, it increases from 700 to 800 °C and then remains practically constant for the C1-TS. On the contrary, the band widths are constant up to 900 °C for C2-Fe while they decrease for the highest temperature. In the present case, the band width is mainly affected by the nanocrystal size and the size distribution. (iv) The $A(D)/A(G)$ intensity ratio (or the crystallite size L_a) drastically increases (decreases) from 700 to 800 °C and remains constant for higher temperatures.

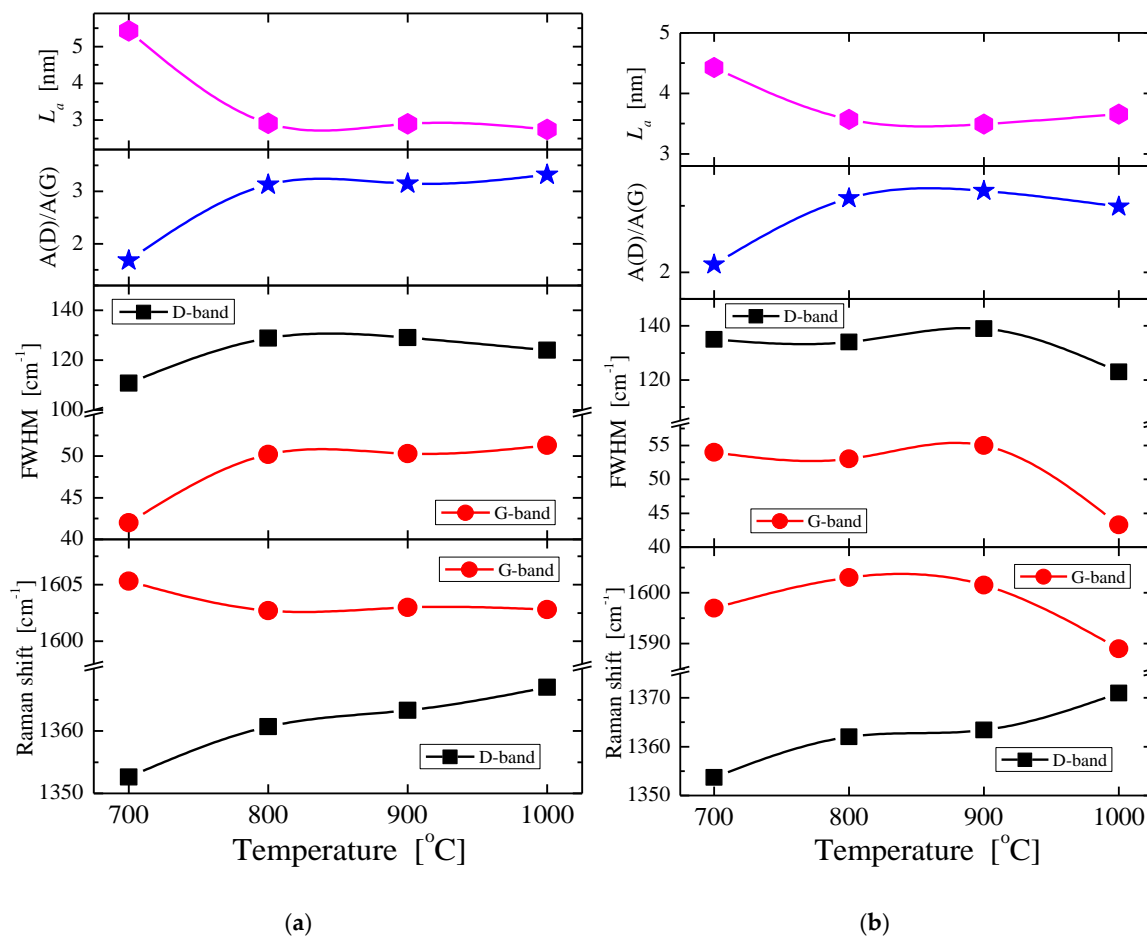


Figure 8. Variation of the Raman spectra fit parameters of (a) C1-TS and (b) C2-Fe vs. temperature. From bottom to top: D and G bands' frequencies, D and G bands' full widths, area ratios, and crystallite size. The lines are drawn as guides to the eye.

3.5. Gas Permeation Measurements

The performance of the two carbon membranes (C1-TS and C2-Fe) was evaluated by single gas permeation measurements of H₂, CH₄ and CO₂ using the Wicke–Kallenbach method. Gas permeation measurements of H₂, CO₂ and CH₄ were performed after each cycle of dip-coating/pyrolysis for both samples. The pyrolysis temperature for the initial cycles was 500 °C and was increased stepwise to 700, 800, 900 or 1000 °C in successive cycles. This carbonization scheme was selected based on results of preliminary experiments, which showed that initial carbonization of membranes with few layers at temperatures higher than 500 °C (600–900 °C) leads to membranes with inferior characteristics (lower selectivity) than the ones prepared with initial carbonization at 500 °C. When a switch to higher pyrolysis temperature was made, the membrane was subjected to treatment at the higher pyrolysis temperature without prior additional dip-coating. The results are presented in Figures 9 and 10 for the permeance of H₂, CH₄ and CO₂ and the ideal H₂/CH₄ and H₂/CO₂ selectivity of the C1-TS membrane. The results are also provided in tabulated form in Table S1. The permeance of the blank support tube was of the order of 10⁻⁵ mol m⁻² s⁻¹ Pa⁻¹. Deposition of the initial eight membrane layers, which were pyrolyzed at 500 °C, leads to a decrease in the permeance by more than two orders of magnitude, which is not accompanied by an appreciable increase in selectivity. Deposition of four additional layers prepared via pyrolysis at 700 °C leads to H₂/CH₄ selectivity higher than 70 and H₂/CO₂ selectivity around 15. Subsequent deposition of additional layers accompanied by an increase in pyrolysis temperature to 800 and 900 °C leads to a further decrease in permeance without a concomitant increase in selectivity, at least for the H₂/CH₄ pair, while the H₂/CO₂ selectivity

attains values around 40. The increase in pyrolysis temperature to 1000 °C causes additional reduction of selectivity to values < 10.

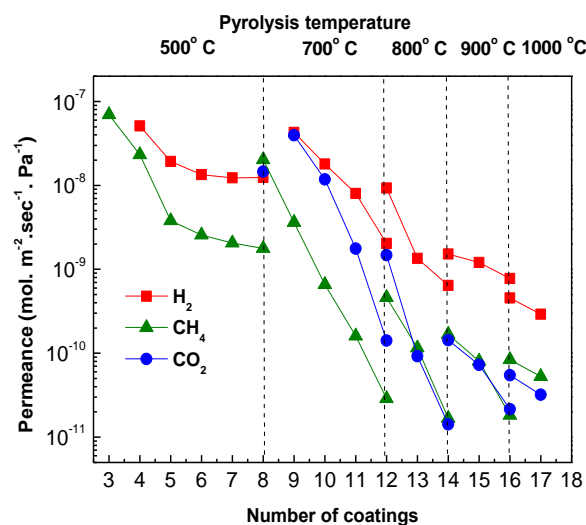


Figure 9. Permeance of H_2 , CH_4 and CO_2 as a function of number of coatings after pyrolysis at 500 °C, 700 °C, 800 °C, 900 °C or 1000 °C for the C1-TS membrane.

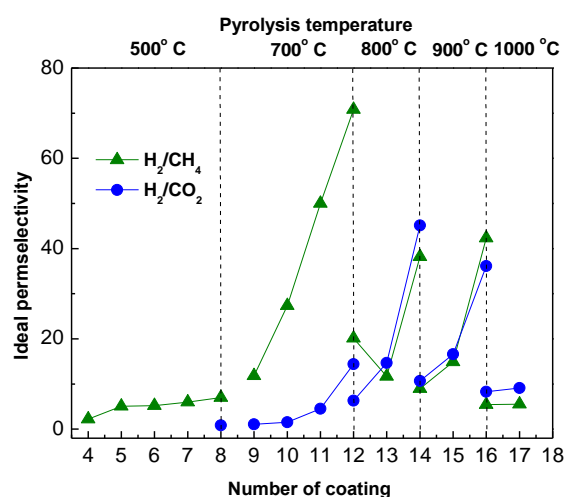


Figure 10. Corresponding H_2/CO_2 and H_2/CH_4 ideal selectivities for the results of Figure 9, C1-TS membrane.

Figures 11 and 12 present the results for the permeance of H_2 , CH_4 and CO_2 and ideal H_2/CH_4 and H_2/CO_2 selectivity, respectively, of the C2-Fe membrane. The results are also provided in tabulated form in Table S2. Deposition of the initial eight membrane layers that were pyrolyzed at 500 °C leads, similarly to the C1-TS membrane, to a decrease in the permeance by more than two orders of magnitude, which is accompanied by an increase in H_2/CH_4 selectivity to 34, while the H_2/CO_2 selectivity is only 2. After pyrolysis at 700 °C without additional coating, the CH_4 permeance increased approximately two orders of magnitude. Deposition of four additional layers with pyrolysis at 700 °C leads to H_2/CH_4 selectivity of 38 and H_2/CO_2 selectivity less than 10. Subsequent deposition of additional layers with pyrolysis at 800 and 900 °C leads to further decreases in permeance without concomitant increases in selectivity, with the exception of the membrane #18, for which permselectivities increased to $H_2/CH_4 = 35$ and $H_2/CO_2 = 58$. The increase in pyrolysis temperature to 1000 °C leads to the loss of membrane selectivity.

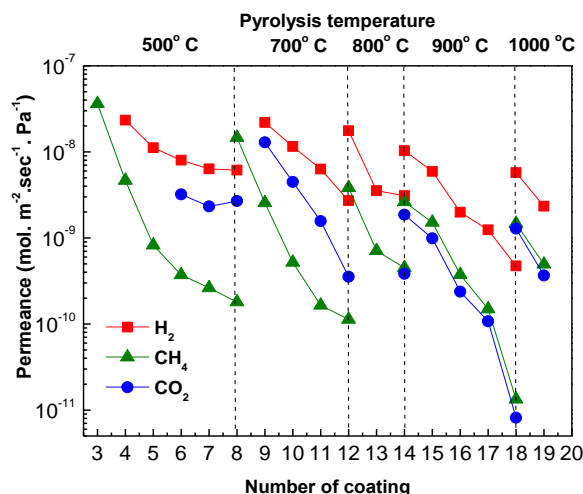


Figure 11. Permeance of H₂, CH₄ and CO₂ as a function of number of coatings after pyrolysis at 500 °C, 700 °C, 800 °C, 900 °C or 1000 °C for sample C2-Fe.

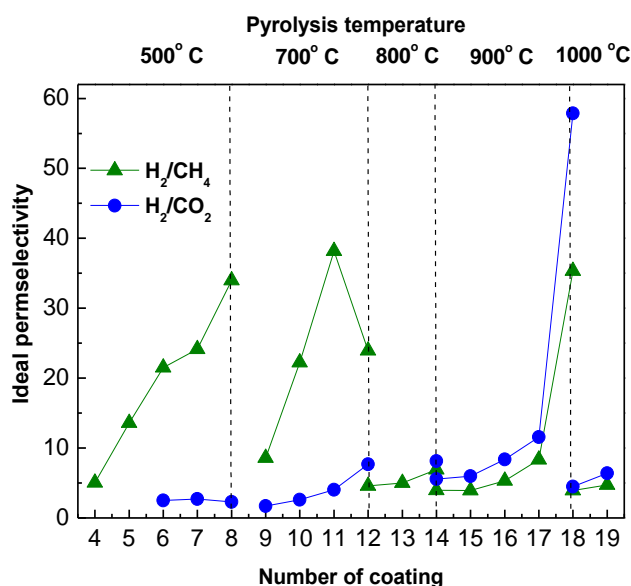


Figure 12. Corresponding H₂/CO₂ and H₂/CH₄ ideal selectivities for the results of Figure 11, C2-Fe membrane.

The effect of permeation temperature on permeation characteristics of C1-TS#16 and C2-FE#18 membranes is depicted in Figures 13 and 14 for H₂, CO₂ and CH₄ permeance, and H₂/CH₄ and H₂/CO₂ selectivity, respectively. The specific membranes were among the ones that showed favorable selectivity results. The gas permeation order for sample C1-TS#16 is H₂ > CO₂ > CH₄ whereas for sample C2-FE#18 is H₂ > CH₄ > CO₂. H₂ permeance increases slightly with temperature for both membranes, indicating an activated diffusion mechanism. The permeance of CO₂ and CH₄ seems to remain unaffected by the permeation temperature for the C1-TS#16 membrane, while it appears to increase slightly with temperature in the case of the C2-FE#18 membrane. The ideal H₂/CH₄ selectivities increase with temperature for both samples, and the same applies for H₂/CO₂ in sample C1-TS#16.

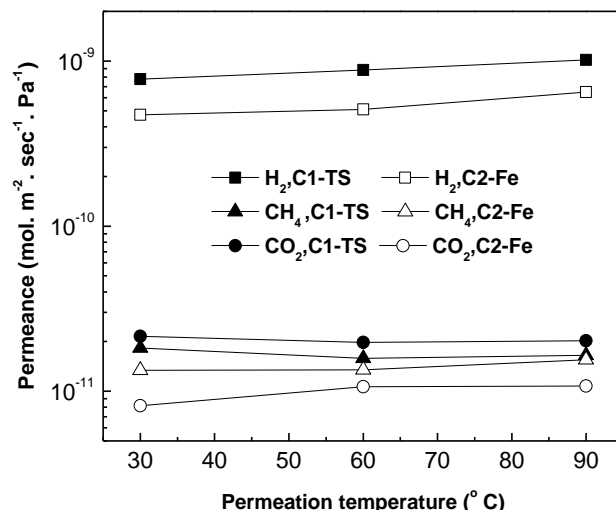


Figure 13. H₂, CH₄ and CO₂ permeance as a function of permeation temperature for sample C1-TS#16 (close symbols) and C2-Fe#18 (open symbols).

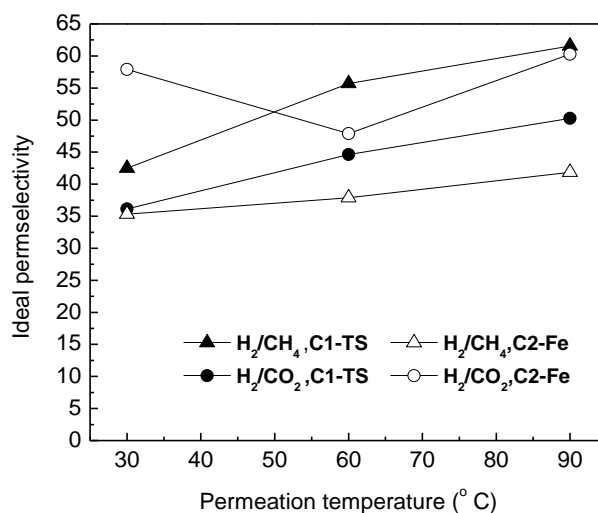


Figure 14. Corresponding ideal H₂/CH₄ and H₂/CO₂ selectivities for the results of Figure 13.

4. Discussion

p-Toluenesulfonic acid (pTS) is a typical acidic polymerization catalyst commonly employed for the preparation of furfuryl alcohol/furfural-based resins, which decomposes during resin pyrolysis. FeCl₃ is also an acidic polymerization catalyst (Lewis-type), which is transformed first to iron oxides and finally to metallic iron during resin pyrolysis. Iron particles catalyze graphitization of amorphous carbon and get encapsulated by the formed graphite-like layers. The main goal of the present work was to examine whether the presence of iron particles surrounded by graphite-like layers could have an appreciable effect on the permeation characteristics of the resulting carbon membranes [21]. The materials characterization confirmed that in-situ formed iron particles enhance the formation of nanocrystalline graphite domains, as evidenced by XRD and Raman spectroscopy. Iron appears also to facilitate the development of carbon mesoporosity, leading to carbon materials with higher specific surface area and pore volume. The highly irreversible nature of nitrogen adsorption at 77 K, especially for the carbon from pTS-catalyzed resin, is indicative of the presence of ultra-small micropores with size comparable to that of the nitrogen molecule.

It was observed that deposition of a considerable number of carbon layers is needed before a measurable increase in selectivity is developed. Even then, the increase in pyrolysis temperature led to additional desorption of gaseous pyrolysis products and restructuring of membrane structure,

causing a decrease in selectivity and an increase in permeance. The separation of the studied molecules takes place mainly via the molecular sieving mechanism and the gas permeation order is $H_2 > CO_2 > CH_4$. However, deviations from the aforementioned order appear in specific cases due to the influence of additional mechanisms, like surface or Knudsen diffusion. In the case of the C1-TS membrane after pyrolysis at 500 °C, for example, the H_2 permeance is equal to that of CO_2 and this behavior is attributed to the contribution of CO_2 surface diffusion mechanism. It is also shown in Figure 10 that methane permeance is higher than the one of CO_2 for the membrane with 13, 14 or 15 coatings. This behavior is attributed to Knudsen diffusion originating from defects in the membrane structure, which favor the permeation of the lighter methane molecule. In the case of the C2-Fe membrane, gas separation takes place mainly via the molecular sieving mechanism. Similarly to the C1-TS membrane, there are instances where the CO_2 permeance is smaller than that of CH_4 , indicating Knudsen diffusion through mesopores or defects on the membrane layer. The overall membrane performance is compared to previous reports in Table 4. Both C1-TS and C2-Fe membranes show inferior behavior to previously reported results regarding H_2/CH_4 selectivity, whereas selectivity values of 402 [11], 617 [13], and 1333 [12] have been reported combined with hydrogen permeance values up to $255 \times 10^{-10} \text{ mol m}^{-2} \text{ s Pa}^{-1}$. On the other hand, the reported H_2/CO_2 selectivities in this work are higher than those reported in the literature.

Table 4. Comparison of H_2 , CO_2 and CH_4 permeance and corresponding H_2/CH_4 and H_2/CO_2 selectivity of C1-TS and C2-Fe membranes with references from the literature.

Membrane	Pyrolysis Temperature (°C)	Permeance ($\times 10^{-10} \text{ mol m}^{-2} \text{ s Pa}^{-1}$)			Ideal Selectivity		Ref.
		H_2	CO_2	CH_4	H_2/CH_4	H_2/CO_2	
C1-TS-#12	700	20.4	1.42	0.29	70.80	14.38	This work
C1-TS-#14	800	6.41	0.14	0.17	38.20	45.13	This work
C2-Fe-#18	900	4.72	0.082	0.13	35.31	57.88	This work
M1	600	255	58.2	0.6	402	4.38	[11]
M2	600	60.4	26.7	0.33	185	2.26	[11]
C/CMS	600	68.29	6.22	0.064	1067	10.98	[12]
C/CMS	900	9.33	1.18	0.007	1333	7.90	[12]
SNPCM-43	450	25.6	1.87	0.0415	617	13.69	[13]

5. Conclusions

$FeCl_3$ is an efficient Lewis acid-type catalyst for polymerization of furfuryl alcohol/furfural mixtures, which is transformed into iron particles during pyrolysis of poly(furfuryl alcohol–furfural) resins and catalyzes the partial transformation of amorphous carbon to graphite, as confirmed by XRD and Raman spectroscopy. The induced changes in carbon structure do not manifest themselves in an improved membrane separation performance for H_2 , CO_2 and CH_4 compared to a carbon membrane prepared using p-toluenesulfonic acid as polymerization catalyst for preparation of the precursor.

Supplementary Materials: The Supplementary Materials are available online at <http://www.mdpi.com/2311-5629/6/3/53/s1>.

Author Contributions: Conceptualization, T.I.; methodology, T.I.; formal analysis, S.N.Y.; investigation, A.Z.; data curation, A.Z.; writing—original draft preparation, A.Z.; writing—review and editing, T.I., S.N.Y.; supervision, T.I. All authors have read and agreed to the published version of the manuscript.

Funding: This research was funded by FCH JU, grant number 278538.

Conflicts of Interest: The authors declare no conflict of interest. The funders had no role in the design of the study; in the collection, analyses, or interpretation of data; in the writing of the manuscript, or in the decision to publish the results.

References

1. Saufi, S.M.; Ismail, A.F. Fabrication of carbon membranes for gas separation. *Carbon* **2004**, *42*, 241–259. [[CrossRef](#)]
2. Sazali, N. A review of the application of carbon-based membranes to hydrogen separation. *J. Mater. Sci.* **2020**, *55*, 11052–11070. [[CrossRef](#)]
3. Foley, H.C. Carbogenic molecular sieves: Synthesis, properties and applications. *Microporous Mater.* **1995**, *4*, 407–433. [[CrossRef](#)]
4. Rao, M.B.; Sircar, S. Nanoporous carbon membranes for separation of gas mixtures by selective surface flow. *J. Membr. Sci.* **1993**, *85*, 253–264. [[CrossRef](#)]
5. Briceno, K.; Garcia-Valls, R.; Montane, D. State of the art of carbon molecular sieves supported on tubular ceramics for gas separation applications. *Asia-Pac. J. Chem. Eng.* **2010**, *5*, 169–178. [[CrossRef](#)]
6. Tanco, M.A.L.; Tanaka, D.A.P. Recent Advances on Carbon Molecular Sieve Membranes (CMSMs) and Reactors. *Processes* **2016**, *4*, 29. [[CrossRef](#)]
7. Anderson, C.J.; Pas, S.J.; Arora, G.; Kentish, S.E.; Hill, A.J.; Sandler, S.I.; Stevens, G.W. Effect of pyrolysis temperature and operating temperature on the performance of nanoporous carbon membranes. *J. Membr. Sci.* **2008**, *322*, 19–27. [[CrossRef](#)]
8. Sanchez, R.; Hernandez, C.; Keresztury, G. Structural analysis of acid catalysed furfuraldehyde resins by thermal degradation techniques. *Eur. Polym. J.* **1994**, *30*, 43–50. [[CrossRef](#)]
9. Fitzer, E.; Schafer, W. The effect of crosslinking on the formation of glasslike carbons from thermosetting resins. *Carbon* **1970**, *8*, 353–364. [[CrossRef](#)]
10. Sedigh, M.G.; Onstot, W.J.; Xu, L.; Peng, W.L.; Tsotsis, T.T.; Sahimi, M. Experiments and Simulation of Transport and Separation of Gas Mixtures in Carbon Molecular Sieve Membranes. *J. Phys. Chem. A* **1998**, *102*, 8580–8589. [[CrossRef](#)]
11. Wang, H.; Zhang, L.; Gavalas, G.R. Preparation of supported carbon membranes from furfuryl alcohol by vapor deposition polymerization. *J. Membr. Sci.* **2000**, *177*, 25–31. [[CrossRef](#)]
12. Song, C.; Wang, T.; Wang, X.; Qiu, J.; Cao, Y. Preparation and gas separation properties of poly(furfuryl alcohol)-based C/CMS composite membranes. *Sep. Purif. Technol.* **2008**, *58*, 412–418. [[CrossRef](#)]
13. Shiflett, M.B.; Foley, H.C. On the preparation of supported nanoporous carbon membranes. *J. Membr. Sci.* **2000**, *179*, 275–282. [[CrossRef](#)]
14. Hussein, M.Z.; Tarmizi, R.S.H.; Zainal, Z.; Ibrahim, R.; Badri, M. Preparation and characterization of active carbons from oil palm shells. *Carbon* **1996**, *34*, 1447–1454. [[CrossRef](#)]
15. Cepollaro, E.M.; Domenico Caputo, D.; Stefano Cimino, S.; Nicola Gargiulo, N.; Lisi, L. Synthesis and Characterization of Activated Carbon Foam from Polymerization of Furfuryl Alcohol Activated by Zinc and Copper Chlorides. *C-J. Carbon Res.* **2020**, *6*, 45. [[CrossRef](#)]
16. Ferrari, A.C.; Robertson, J. Interpretation of Raman spectra of disordered and amorphous carbon. *Phys. Rev. B* **2000**, *61*, 14095–14107. [[CrossRef](#)]
17. Dresselhaus, M.S.; Dresselhaus, G.; Saito, R.; Jorio, A. Raman spectroscopy of carbon nanotubes. *Phys. Rep.* **2005**, *409*, 47–99. [[CrossRef](#)]
18. Tuinstra, F.; Koenig, J.L. Raman spectrum of graphite. *J. Chem. Phys.* **1970**, *53*, 1126–1130. [[CrossRef](#)]
19. Cancado, L.G.; Takai, K.; Enoki, T.; Endo, M.; Kim, Y.A.; Mizusaki, H.; Jorio, A.; Coelho, L.N.; Magalhaes-Paniago, R.; Pimenta, M.A. General equation for the determination of the crystallite size L_a of nanographite by Raman spectroscopy. *Appl. Phys. Lett.* **2006**, *88*, 163106. [[CrossRef](#)]
20. Wang, Z.; Lu, Z.; Huang, X.; Xue, R.; Chen, L. Chemical and crystalline structure characterizations of polyfurfuryl alcohol pyrolyzed at 600 °C. *Carbon* **1998**, *36*, 51–59. [[CrossRef](#)]
21. Kicinski, W.; Norek, M.; Bystrzejewski, M. Monolithic porous graphitic carbons obtained through catalytic graphitization of carbon xerogels. *J. Phys. Chem. Solids* **2013**, *74*, 101–109. [[CrossRef](#)]

